Numerical investigation of the effects of porosity and tortuosity on soil permeability using coupled three-dimensional discrete-element method and lattice Boltzmann method

Bahman Sheikh* and Ali Pak†
Department of Civil Engineering, Sharif University of Technology, Tehran, Iran
(Received 27 October 2014; revised manuscript received 15 February 2015; published 11 May 2015)

Permeability of porous materials is an important characteristic which is extensively used in various engineering disciplines. There are a number of issues that influence the permeability coefficient among which the porosity, size of particles, pore shape, tortuosity, and particle size distribution are of great importance. In this paper a C++ GPU code based on three-dimensional lattice Boltzmann method (LBM) has been developed and used for investigating the effects of the above mentioned factors on the permeability coefficient of granular materials. Multirelaxation time collision scheme of the LBM equations is used in the simulator, which is capable of modeling the exact position of the fluid-solid interface leading to viscosity-independent permeabilities and better computational stability due to separation of the relaxations of various kinetic models. GPU-CPU parallel processing has been employed to reduce the computational time associated with three-dimensional simulations. Soil samples have been prepared using the discrete element method. The obtained results have demonstrated the importance of employing the concept of effective porosity instead of total porosity in permeability relationships. The results also show that a threshold porosity exists below which the connectivity of the pores vanishes and the permeability of the soils reduces drastically.

DOI: 10.1103/PhysRevE.91.053301 PACS number(s): 02.60.−x, 81.05.Rm, 47.56.+r, 47.15.G−

I. INTRODUCTION

The prediction of the permeability of porous media has been a challenge for engineers and scientists because of its essential role in solving problems of seepage, drainage, consolidation and its application in the industry. For instance, knowledge of flow through a porous material is required for a good understanding of problems in oil recovery, the flow of groundwater, and contaminant transport in aquifers. Permeability is defined as the process of transfer of fluid, gas, or solutes through porous media which is governed mainly by the porous media's structure or the geometry of pore space in porous media, which is considered to be the key in understanding of this process. However, a quantitative and explicit characterization by means of a physical interpretation is difficult because of the complexity of the pores shapes and pore connectivities. It has been an old challenge to scientists to relate the direct features of porous media to permeability without conducting expensive or time-consuming experiments. The experimental methods used in the studies have varied from rather straightforward measurements [1–4] to sophisticated approaches, which utilize, for example, mercury porosimetry, electrical conductivity, nuclear magnetic resonance, acoustic properties of the medium, also using constant or variable head permeameter [4–10] for measuring the permeability. Theoretical works have often involved models with simplified pore geometries, which allows development of analytical solutions for microscopic flow patterns [11–13]. More sophisticated theoretical models based on statistical methods have also been used [1,12,13]. However, due to the extremely complex nature of the phenomena, many basic questions have remained unanswered. Following such a morphological path, the characterization of the geometrical properties of the soil structure should be quantitative to allow the results to be incorporated into the analyses. As another requirement, the interpretation of the results towards the physics of the processes should be possible. The latter was critical in the previous attempts of relating soil structure and the developed function [14,15].

The typical problem of the permeability of porous media emerges when considering saturated flow of water in soil. The intrinsic permeability of the soil can be determined by the arrangement of the solid particles, the pores, and solid space geometry. One important geometrical aspect is the distribution of the pore volume over a range of effective pore diameters which corresponds to the hydraulic diameter according to the capillary rise equation. For precise description of fluid flow through soil and computing the permeability of a given medium, if one knows the structure of the medium, a combination of Newton's second law with the Navier-Stokes equations of hydrodynamics can be used. Having determined the steady-state velocity field for a given pressure gradient one then has the mean flow velocity and hence the permeability. Unfortunately, neither of these two steps is necessarily easy. Most porous media of practical interest have extremely complex three-dimensional (3D) geometries that are difficult to be determined in detail. Assuming that some way can be found for determining the geometry of the solid matrix, solving the Navier-Stokes equations in the presence of highly irregular solid-fluid boundaries has proved to be a difficult task. As a result, obtaining purely theoretical formulae is very cumbersome and thus impractical for normal engineering problems. Therefore, engineers often follow the simpler empirical method given by Darcy's law, which says that as long as we consider saturated flow at a low Reynolds number, the mean flow rate of a viscous fluid through a porous medium is proportional to the applied pressure difference and inversely proportional to the viscosity. Darcy's law is valid

*Corresponding author: Bahman Sheikh, Department of Civil Engineering, Sharif University of Technology, Tehran, Iran; sheikh.bahman@gmail.com
†pak@sharif.edu

for laminar flow through porous media, which is found to be applicable to a wide range of soil types, from clays to coarse sands. The general 3D form of Darcy's law is as follows [16]:

$$v_i = \frac{k_{ij}}{\nu}\frac{\partial P}{\partial x_j} = K_{ij}\frac{\partial P}{\partial x_j}, \quad i, j = 1, 2, 3, \tag{1}$$

where v_i is discharge velocity in direction i,k_{ij} is intrinsic permeability, K_{ij} is hydraulic conductivity matrix, ν is dynamic viscosity, P is applied pressure, and x_j is distance in direction j. It is well known that independent estimates of hydraulic conductivity are not, in general, very reliable [17–19]. The hydraulic conductivity value may be either assessed using predictive methods or measured using laboratory or field testing. The objective of predictive methods is most often to reduce the cost of tests; however, they usually give a rough prediction of hydraulic conductivity value [17]. In many instances, attention should be paid to correct estimation of k. Because an examination of Eq. (1) shows that the intrinsic permeability has units of length squared. On the reasonable assumption that this length will be something typical of the system under study, it is clear that the permeability is a quantity that can vary enormously, and no other property of importance in geotechnical problems is likely to exhibit such a great range of values, up to 10 orders of magnitude, from coarse to very fine-grained soils [20].

As mentioned, many factors affect the hydraulic conductivity of granular soils such as soil structure, fluid physical properties, and degree of fluid saturation. However, the focus of this study is on the effects of soil structure on the soil permeability. Conventional predictive relationships are usually correlations between intrinsic permeability and porosity. Other than this, there are also some factors that have major influences on soil permeability such as specific surface of particles, shape of particles, and tortuosity; a number of them are included in some correlations. Statistical models for the permeability of soil are based on the distribution of pore sizes [21,22]. But the models should include matching parameters defined as connectivity and tortuosity. Without these factors the pore size distribution models would just mimic the permeability of a bundle of straight capillary tubes. However, the reality in a soil is much more complex, with twisted and crooked pores that are dead-end or connecting to other pores. This means that there is a need to scale down the permeability to the capillary tube model to include the increased path length due to crookedness of the path (tortuosity) or considering the lack of connection between certain points in the soil (connectivity). Although there are some approaches available for estimating specific surface of granular soils, direct measurements of tortuosity, connectivity, and shape factor from usual laboratory tests are difficult. Due to the complexity of flow in porous media, pure analytical solutions cannot be obtained except for very few problems such as fluid flow through a cubic array of spheres of equal radius [23,24]. Recently, numerical simulation of fluid flow through porous media at the pore scale has been of interest. Because of the complexity of the pore geometry, most of the previous pore-scale simulations of fluid movement in soils were based on simplifications that idealized the complicated soil structures into models such as fractal structures [25] and network models [26]. Simulations based on those idealizations provides insight into the pore-scale fluid movement and some of network models are even able to include topological features, but it is not easy to obtain the geometrical parameters to construct the ideal soil structure that has to be hydraulically equivalent to the real soil [27]. In the past few decades with rapid development of techniques of visualization and quantification of pore geometry of porous media, the increase of computational power and the advances in fluid modeling capacities, direct simulation of pore-scale water movement in soils without idealizing the pore geometry has been feasible [27]. Therefore, fluid flow simulation at pore level has received considerable attention as a powerful tool for the permeability prediction.

One of the numerical methods which seem ideal for simulating fluid flows in complicated geometries such as particulate media is lattice Boltzmann method (LBM) [28]. LBM was applied to porous media flow soon after its emergence in Ref. [29]. The geometrical versatility of this method makes it particularly useful for simulating flows in irregular geometries [30–34]. Later studies confirmed the reliability of LBM in modeling seepage around solid particles [35,36]. Heijs and Lowe [37] investigated the flow in a random array of spheres and a clay soil sample using the LBM. They used the bounce-back scheme for modeling the solid wall boundary condition and found that the LBM yields acceptable results even with very coarse lattice. Most of the conducted research using LBM has been two-dimensional (2D) endeavors.

In this paper, a multirelaxation time 3D lattice Boltzmann numerical simulation of fluid flow through a soil pack comprising spherical rigid particles is considered. Packing of particles with certain grading distribution characteristics was created by a random particle generator and isotropic compression technique using the discrete element method (DEM). By using this numerical approach, correlations between various macroscopic parameters such as porosity, effective porosity, specific surface area, tortuosity, and particle size distribution with intrinsic permeability for monosized and multisized samples were investigated. The variation of permeability near the percolation threshold was also analyzed. Since 2D simulations cannot consider the real spatial pore connectivities and 3D flow paths, 3D simulations have been carried out throughout this research.

II. POROUS MEDIA

A. Permeability

A number of methods for predicting intrinsic permeability of soils can be found in the literature. Among all methods, a general relationship which is known as the KC equation was first proposed by Kozeny as [38]

$$k = \frac{\phi^3}{cS^2}, \tag{2}$$

where ϕ is the soil porosity and S is the specific surface area, and c is the Kozeny coefficient. One of the most widely accepted attempts to generalize Eq. (2) was proposed by Carman [39,40] who noticed that the streamlines in a porous medium are far from being straight and parallel to each other. This effect can be described by a dimensionless parameter T

called hydraulic tortuosity [41]:

$$T = \frac{\langle \lambda \rangle}{L} \geqslant 1, \tag{3}$$

where $\langle \lambda \rangle$ is the average length of the fluid paths and L is the geometrical length of the sample. Using the tortuosity, Kozeny's equation can be generalized to [42]

$$k = \frac{\phi^3}{cT^2S^2}. \tag{4}$$

By fitting the experimental data, Carman concluded that T^2 is a constant factor over a wide range of porosities. Later it was found that T^2 does vary with ϕ. However, considering flow through a porous medium, only the interconnected pores are of interest, as the occluded pores (pores not connected to the main void space) do not contribute to the flow. The dead-end pores are another type of pores that contribute very little to the flow. These pores belong to the interconnected pores, but, owing to their geometry, no global path lines intersect them. The occluded pores and the dead-end pores form the no conducting pore space of the medium. The effective porosity ϕ_{eff} of a porous medium can be defined as the ratio of the volume of the conducting pores to the total pore volume [43]. In the porous media with high porosity, all of the void spaces usually contribute to the flow. The effective porosity of the medium is then equal to the porosity. On the contrary, for low-porosity materials, a large part of the total void space may be no conducting. For such media the effective porosity may, therefore, be significantly smaller than the geometrical porosity. At the percolation threshold ϕ_c, defined as the point where the medium becomes completely blocked, permeability and effective porosity both vanish. It is therefore clear that the KC equation, as given by Eq. (4), is not valid when $\phi \to \phi_c$. The simplest way to modify Eq. (4) to include the effect of no conducting pores is to replace the porosity ϕ with the effective porosity ϕ_{eff}. So, as Ref. [43] proposed we can obtain

$$k = \frac{\phi_{\text{eff}}^3}{cT^2S^2}. \tag{5}$$

Assuming spherical particles, and substituting for S in Eq. (4) leads to

$$k = \frac{\phi^3}{36cT^2(1-\phi)^2}d_p^2, \tag{6}$$

where d_p is the particle diameter, and $c = 2.5$ is given for beads of spherical particles [44]. Carman proposed a constant tortuosity of $T = \sqrt{2}$ based on his experimental measurements of permeability [39]. As a result, the widely used form of the KC correlation for monosized sphere packing is obtained as [16]

$$k = \frac{\phi^3}{(1-\phi)^2}\frac{d_p^2}{180}. \tag{7}$$

This is considered as a simple, yet practical, correlation for expressing the permeability of granular media in terms of particle size and porosity. If we substitute ϕ by ϕ_{eff} in Eq. (7) we obtain

$$k = \frac{\phi_{\text{eff}}^3}{(1-\phi_{\text{eff}})^2}\frac{d_p^2}{180}. \tag{8}$$

Bear and Bachmat [45] proposed another equation, which for comparison purposes after some substitutions becomes

$$k = \frac{1-1.209(1-\phi)^{2/3}}{60\phi}\frac{\phi^3}{(1-\phi)^2}d_p^2. \tag{9}$$

Recently, Ahmadi *et al.* [46] by analytical derivation provided the following relationship:

$$k = \frac{1-1.209(1-\phi)^{2/3}}{30[1-1.209(1-\phi)^{2/3}+2\phi]}\frac{\phi^3}{(1-\phi)^2}d_p^2. \tag{10}$$

It can be concluded from the above relations that the effective porosity, tortuosity, and particles' diameter or specific surface of particles have great influence on the permeability of porous media.

B. Tortuosity

As mentioned, tortuosity is defined as the ratio of an average length of microscopic flow paths to the length of the soil sample in the direction of the macroscopic flux [Eq. (3)]. The tortuosity of the packed media is rarely a constant value; rather, it varies according to the factors related to the motion of fluid coupled with certain geometrical characteristics of the packing. Tortuosity is always greater than one and decreases with increasing the porosity, so that as the porosity approaches one, the tortuosity also tends to unity. There is a large scatter in the existing tortuosity correlations, especially in their form and their range of applicability due to porosity. Some of the tortuosity functions available in the literature are as follows.

Koponen *et al.* [47] studied the permeability and tortuosity of 2D random porous media using the lattice gas automata. The tortuosity was correlated with porosity as a linear relationship as follows:

$$T = p(1-\phi) + 1, \tag{11}$$

where p is a fitting parameter. Later they found that this relation is not consistent with the results obtained for the porosity range $0.4 < \phi < 0.5$, and suggested [43] to replace it with

$$T = p\frac{1-\phi}{(\phi-\phi_c)^m} + 1, \tag{12}$$

in which $\phi_c \approx 0.33$ was used as the percolation threshold and p and m are empirical parameters.

Weissberg [48] proposed the below relation:

$$T = 1 - 0.40\ln(\phi), \tag{13}$$

which was later validated empirically [49]. Du Plessis and Masliyah [50] provided the following analytical function for isotropic granular media based on the concept of a representative unit cell:

$$T = \frac{\phi}{1-(1-\phi)^{2/3}}. \tag{14}$$

Boudreau [51] has proposed this empirical equation:

$$T = \sqrt{1-\ln(\phi^2)}. \tag{15}$$

The Comiti and Renaud [52] relation is as follows:

$$T = 1 - p\ln(\phi). \tag{16}$$

Ref. [53] suggested the following equation:

$$T = \sqrt{1 + 2(1 - \phi)}. \tag{17}$$

In a recent attempt, Ref. [46] proposed an equation based on analytical derivation as follows:

$$T = \sqrt{\frac{2\phi}{3\left[1 - 1.209(1 - \phi)^{\frac{2}{3}}\right]}} + \frac{1}{3}. \tag{18}$$

Besides all of these functions Refs. [42,54–56] proposed similar simple function as follows:

$$T = \frac{1}{\phi^p}, \tag{19}$$

where p is a fitting parameter.

Although most of the above correlations are validated in conductivity experiments and are highly accredited by several researchers, they have very different mathematical forms. The same inconsistency is observed for correlations derived from numerical simulations. Reference [57] suggested a correlation of the form given by Eq. (11) from 2D simulations using the LBM, while similar numerical simulations in Ref. [41] showed a correlation of the form $1 + ln\phi$, which is different from Eq. (11). Besides all of this, one thing seems obvious, that the 2D numerical simulations cannot adequately account for tortuosity variations. Due to the 3D nature of tortuosity, it may not be limited to in-plane flow paths. However, since the 3D numerical flow simulations are usually computationally cumbersome, they have rarely been used in the literature.

III. NUMERICAL TECHNIQUES

A. Lattice Boltzmann method (LBM)

Conventional techniques such as finite elements use prefixed laws to calculate fluid flux or pressure. The laws usually are derived from the Navier-Stokes equation via some simplifying assumptions such as homogenization and empirical modifications. These methods have some uncertainty for investigating phenomena such as fluid flow in porous media because of the nature of assumptions and parameters.

During the last two decades, particle-based methods such as lattice Boltzmann have been developed as a robust numerical approach in computational fluid dynamics. LBM, which numerically solves the Navier-Stokes equation in a general condition, has emerged as a powerful alternative tool for simulation of fluid flows. Its strength lies in the ability to easily represent complex physical phenomena. The method finds its origin in a molecular description of fluid and can directly incorporate physical terms stemming from knowledge of the interaction between molecules. For this reason, it is an invaluable tool for fundamental research, as it keeps the cycle between the elaboration of a theory and the formulation of its corresponding numerical model short. On the other hand, a distinct advantage of the LBM in geotechnical problems lies in its capability of modeling problems with complex pore geometry and with a large number of particles such as soil. The fundamental idea of the LBM is to construct simplified kinetic models that incorporate the essential physics of microscopic or mesoscopic processes, so that the microscopic averaged properties obey the desired macroscopic equations [28].

The most popular LBM is Bhatnagar-Gross-Krook (BGK) model [58] with a standard bounce-back (SBB) scheme for fluid–solid boundaries. In BGK the collision operator is approximated by a single-relaxation-time (SRT) approximation, which has some defects such as numerical instability and viscosity dependence of boundary locations, especially in underrelaxed situations [59]. The viscosity-dependent boundary conditions pose a severe problem for simulating flow through porous media because the permeability becomes viscosity dependent, while it should be a characteristic of the physical properties of the porous medium alone. This issue is reported by some authors [41,60]. The deficiencies inherent in the BGK model can be significantly reduced by using a multiple-relaxation-time (MRT) approach [60,61], which separates the relaxation times for different kinetic modes and allows tuning to improve numerical stability and accuracy. In addition, the BGK model may experience numerical instability when simulating elevated Reynolds number flow or when the relaxation time approaches 0.5. One remedy is to increase the grid density to alleviate the excessive reduction of the relaxation time. However, this practice would be impractical due to the substantial increase of the computational effort. An alternative is to adopt the MRT lattice Boltzmann model [62].

The starting point of the formulation is the continuous Boltzmann equation which expresses how the probability $f(x, v, t)$ of finding a particle with velocity v at a position x and at time t evolves with time [62]:

$$\frac{\partial f}{\partial t} + v \cdot \nabla f = \Omega, \tag{20}$$

where f is the single particle density distribution function and Ω is the collision term, and accounts for the change in distribution function due to particle collisions. This continuous Boltzmann equation may be discretized in time and space. Consider the 3D lattice Boltzmann model on a square lattice with lattice spacing δx and 19 discrete lattice velocities in the D3Q19 space discrete model. After discretizing the continuous Boltzmann equation with multirelaxation time collision approximation, it can be written as the following equation. On each lattice site values of 19 density distribution function f_α are stored, each of them assigned to a lattice vector c_α:

$$f_\alpha(r + c_\alpha\delta_t, t + \delta_t) = f_\alpha(r,t) - M^{-1}S[f_\alpha(r,t) - f_\alpha^{\mathrm{eq}}(r,t)]\alpha = 1 - 19, \tag{21}$$

where M is an integer transformation tensor which is designed to contain more physically relevant quantities, e.g., density, momentum, energy, and their fluxes, f_α^{eq} is the equilibrium density distribution function, $r(x, y, z)$ is the space position vector, t denotes time, δ_t lattice time. The transformation tensor M and the functional forms of the equilibrium moments f_α^{eq} for the D3Q19 lattice are given in Refs. [61,63,64]. S is the diagonal relaxation matrix, indicating that the collision process for each moment is accomplished by a linear relaxation towards its equilibrium. The values of the collision parameters correspond to the conserved moments, to determine the shear and bulk viscosities, and to preserve the symmetry on the

chosen lattice:

$$S = \mathrm{diag}(0,\ s_e,\ s_\varepsilon, 0,\ s_q, 0,\ s_q, 0,\ s_q,\ s_\upsilon,\ s_\pi,\ s_\upsilon,$$
$$s_\pi,\ s_\upsilon,\ s_\upsilon,\ s_\upsilon,\ s_m,\ s_m,\ s_m). \tag{22}$$

The values of the collision parameters that correspond to the conserved moments are irrelevant because $f(r,t) = f^{\mathrm{eq}}(r,t)$ and can be anything; here we set them to be zero. In addition, the relaxation rate s_υ, which determines the viscosity υ, is

$$\upsilon = \frac{1}{3}\left(\frac{1}{s_\upsilon} - \frac{1}{2}\right). \tag{23}$$

There are five other relaxation rates that are adjustable parameters: s_e, s_ε, s_π, s_m, and s_q, are set to be identical values to preserve symmetry on the chosen lattice as follows [36,65]:

$$s_e = s_\varepsilon = s_\pi = s_m = s_q = 8\frac{2 - s_\upsilon}{8 - s_\upsilon}. \tag{24}$$

This general model reduces to the usual single-relaxation BGK model if all relaxation parameters are set to be a single value $\tau = 1/s_\upsilon$, i.e., $S_\alpha = 1/\tau$. For more information about the MRT-D3Q19 the interested reader can refer to Refs. [63,64].

A constraint to the parameter selection is that the lattice speed C, defined as $C = \delta_h / \delta_t$, where δ_h is lattice spacing, must be sufficiently larger than the maximum fluid velocity ($\upsilon_{\max}$) in the simulation domain to ensure sufficient solution accuracy. This is controlled by the computational Mach number, defined by

$$\mathrm{Ma} = \frac{\upsilon_{\max}}{C}. \tag{25}$$

Theoretically, it is required that $\mathrm{Ma} \ll 1$. In practice, Ma should be, at least, smaller than 0.1 [66]. This becomes very important in modeling fluid flow through pack of solid particles, when fluid particles may have high velocities in small communications between channels [67].

One of the distinguishing features of LBM is undoubtedly its highly parallelizable data structure. Nowadays scientific computing on graphics processing units (GPUs) has become more important, due to their advantages for scientific calculations. Nevertheless, it has to be noted that there are important differences in architecture and the programming of GPUs and CPUs, based on their historical development and assignment. In order to use the advantages of the architecture of GPUs, lattice-based algorithms are well suited. In this study, a coupled CUDA multi-GPUs and OpenMP code based on 3D (D3Q19) parallel processing version of lattice Boltzmann method has been developed, in order to simulate fluid flow in porous media. As mentioned, a MRT approximation of the LBM equations is used in the simulator.

In order to verify the developed MRT-LBM code and the assumed boundary conditions, first, the Poiseuille flow between two parallel plates is simulated for which analytical solutions can be derived by solving the appropriate Navier–Stokes equation. Between the two plates, the velocities at the plates are zero (no-slip boundaries), and the velocity reaches its maximum in the middle. The velocity profile between two plates of width $2a$ is parabolic given by

$$u(y) = \frac{\Delta p}{2\nu\rho L}(a^2 - y^2) \tag{26}$$

or

$$u(y) = \frac{g}{2\nu}(a^2 - y^2), \tag{27}$$

where L is domain length along the flow direction, ρ is fluid density, ν is fluid dynamic viscosity, Δp is pressure gradient between inlet and outlet of domain, and g is acceleration.

Here we performed two simulations: first, Poiseuille flow driven by pressure gradient (Test-1) and second Poiseuille flow driven by a body force (Test-2). Both simulations have bounce-back [68] boundaries at plates ($y = -a$, $y = a$) and periodic boundaries in the z direction [Fig. 1(a)]. At the Test-1, the inlet and outlet of the domain (x direction) are set to be pressure boundary which is implemented to the code according to Ref. [69]. But in the Test-2, the periodic boundary condition is set for x direction and the pressure gradient was simply applied by adding an equivalent body force ($g \cdot \rho = \Delta p/L$). According to Fig. 1(b) agreement of LBM results with the analytical solution is excellent.

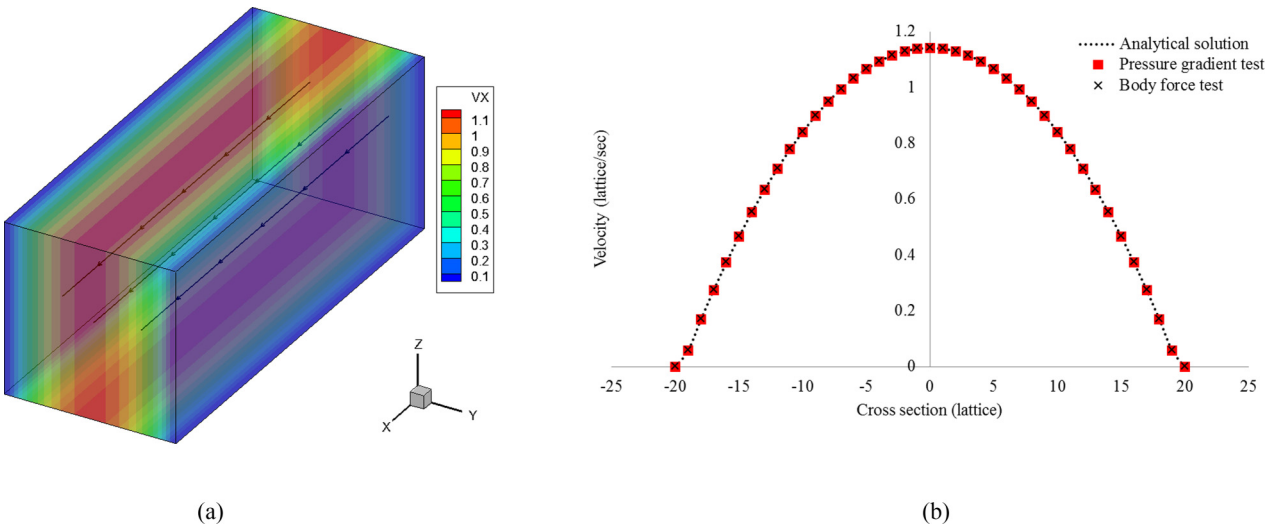

(a) (b)

FIG. 1. (Color online) Poiseuille flow between two parallel plats: (a) velocity contour; (b) velocity profile.

B. Discrete element method (DEM)

DEM is an explicit numerical method for modeling the dynamic behavior of an assembly of distinct objects. The model explicitly reproduces the discrete nature of the discontinuities, which are represented as the boundary of each element. The method has become a powerful numerical tool for analyzing particulate media since it was first introduced by Cundall and Strack [70]. A wide range of problems in different branches of engineering is successfully simulated by DEM. DEM conceives granular materials as an assemblage of distinct rigid particles. The equilibrium contact forces and displacements of a stressed assembly of spheres are found through a series of calculations tracing the movements of individual particles. These movements are the result of the propagation of disturbances in the medium originating at the boundaries. The calculations performed in the DEM alternate between the application of Newton's second law to the particles and a force-displacement law at the contacts. Newton's second law determines motion of a particle resulting from the forces acting on it. The force-displacement law is used to find the contact forces from displacement. This calculation cycle is conducted in each time step during the analysis. For more information about the DEM formulations see Refs. [70–72].

In this study, DEM simulations have been used to numerically generate packed particle samples. Several methods for specimen generation are currently available [71–75]. In this study the random generation approach proposed by Itasca [71] has been employed, which consists of sequentially selecting solid particles according to a given particle size distribution, in descending order of size and positioning them in random coordinates. If a particle does not fit, the radius is retained but another location is randomly chosen. Positioning of each solid particle is attempted a number of times till the new particle is positioned with no overlap with other particles in the domain. In each trial, if the recently created particle has a tiny overlap with a neighboring particle, a small change in the coordinates is applied to the particle, which leads to elimination of the overlap. The coordinate change is repeated quite a number of times to remove all the overlaps, and if these attempts did not work, a new random positioning starts. This approach will generate relatively loose specimens. Generating medium or dense packings by random coordinate generator is very time consuming or even impossible. An effective way to generate denser samples is mechanical packing by DEM. For this purpose an isotropic compression technique is employed. In the isotropic compression method, all solid particles are first randomly positioned in a large area which is bigger than the main domain by a particle filling procedure, so that no overlap exists between the particles. Then the boundary walls are moved inward to compact the assembly until a target porosity value is achieved (Fig. 2). During the isotropic compaction in 3D, six rigid walls move inward simultaneously with a constant low speed. The friction coefficient between particles and walls were set to zero in order to decrease the effects of boundary walls on the results. Also, damping parameters were set to small values, in order to obtain a quick propagation of particle movements from boundary particles through central ones. Porosity measurements in different sections of the generated samples show that these measures have led to creating relatively homogenous samples.

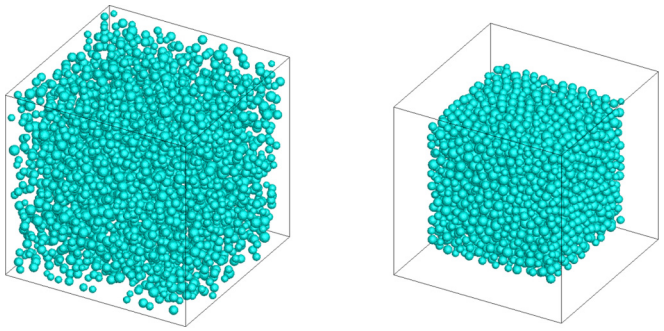

FIG. 2. (Color online) Isotropic compression technique for generating dense samples: (a) before isotropic compaction; (b) after isotropic compaction.

IV. NUMERICAL SIMULATION OF FLOW IN POROUS MEDIA

Each of the generated samples using DEM is introduced to LBM code as an input. One problem with the LBM method is that it is incapable of resolving the macroscopic Navier-Stokes equations for channels narrower than about four lattice units [76]. This limitation becomes particularly important at low porosities, for which the number of very narrow passages increases enormously. To bypass this problem, a standard numerical mesh refinement procedure is used [41]. Then the spherical solid particles are mapped onto a lattice. During fluid flow simulations, solid areas are considered immovable and they interact with fluid particles by the bounce-back boundary rule, which will be describe later.

In this work, lattice spacing is considered 0.01 mm based on the size of the finest particles that exist in the sample and in order to maintain Mach number as low as possible. This leads to relatively large numbers of computational lattices (our simulations contain about $500 \times 500 \times 500$ lattices). For all LBM simulations, a difference in hydraulic head is applied at two opposite sides of the soil sample (inlet and outlet of domain along the x direction; Fig. 3), by means of pressure boundary condition (or density boundary condition $\Delta p = \Delta\rho \cdot C^2$), which is implemented to the code according to [69]. The interface between the solid boundaries and the flowing fluid is assumed to be nonslip. Simulating slip and nonslip boundaries in the LBM is an area where progress is still being made. Among the existing methods, the simplest is called the bounce-back [68] method. In this approach, to ensure that the fluid particles have zero average velocity at the boundaries, any flux of fluid particles that hits a boundary simply reverses its velocity so that the average velocity at the boundary is automatically zero. This type of boundary is utilized in this study for solid lattices. It worth mentioning that the position of a boundary is viscosity dependent when applying the BGK model. One of the methods for tackling this problem is using the MRT model. In this way the viscosity dependence can be eliminated by individually adjusting the

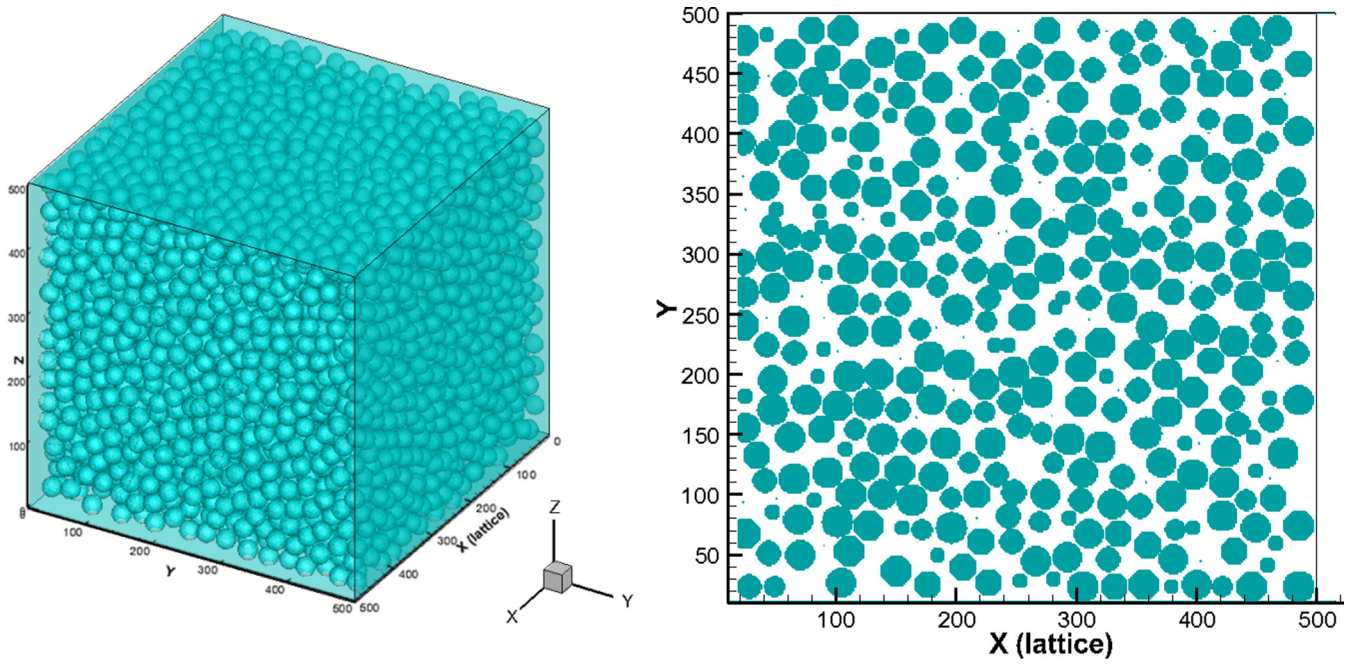

FIG. 3. (Color online) (a) An example of monosized sample generated by DEM and introduced to LBM code. (b) A cross section at $z = 250$ lattice of the 3D sample.

collision parameters [36,65,77]. This feature of MRT will be shown later.

An example of such prepared porous systems is depicted in Fig. 3. The blue areas represent fixed solid obstacles, while the white part is occupied by the fluid. We believe that the homogeneity of the randomly generated samples (with $500 \times 500 \times 500$ lattices) is well satisfied because we have simulated each of the samples at least twice and the results were almost the same. Summary of the grain size distribution characteristics of the generated samples used in this study are reported in Table I and Table II. The grain size distribution curves related to Table II along with an example of non-homogenized sample are depicted in Fig. 4.

Virtual velocity of fluid and tortuous flow paths can be easily traced by LBM. Figure 5 shows a representative illustration of numerical simulation. Only a number of flow paths are depicted on this figure. Herein permeability of the samples of spherical solid particles which can be representative of sandy

TABLE I. Summary of monosized samples characteristics used in this study.

Porosity	Particles diameter (cm)	No. of simulation	Re	Porosity	Particles diameter (cm)	No. of simulation	Re	Porosity	Particles diameter (cm)	No. of simulation	Re
0.5	0.08	3	0.006	0.75	0.08	3	0.183	0.7	0.2	2	0.309
0.5	0.1	3	0.010	0.8	0.08	3	0.316	0.75	0.2	2	0.453
0.5	0.12	4	0.014	0.85	0.08	3	0.585	0.8	0.2	2	0.800
0.5	0.14	3	0.023	0.9	0.08	3	1.170	0.85	0.2	2	1.262
0.5	0.16	3	0.033	0.4	0.12	2	0.000	0.9	0.2	2	2.424
0.5	0.18	3	0.042	0.45	0.12	2	0.004				
0.5	0.2	3	0.056	0.55	0.12	3	0.041				
0.6	0.08	4	0.023	0.6	0.12	2	0.063				
0.6	0.1	4	0.033	0.65	0.12	2	0.099				
0.6	0.12	4	0.059	0.7	0.12	2	0.186				
0.6	0.14	4	0.087	0.75	0.12	2	0.274				
0.6	0.16	4	0.118	0.8	0.12	2	0.480				
0.6	0.18	4	0.162	0.85	0.12	2	0.887				
0.6	0.2	4	0.205	0.9	0.12	2	1.754				
0.4	0.08	3	0.000	0.4	0.2	2	0.001				
0.45	0.08	3	0.002	0.45	0.2	2	0.005				
0.55	0.08	3	0.028	0.55	0.2	2	0.068				
0.65	0.08	4	0.066	0.6	0.2	2	0.104				
0.7	0.08	4	0.124	0.65	0.2	2	0.163				

TABLE II. Characteristics of grain size distribution curves for nonhomogenized samples used in this study.

Curve No.	No. of simulation	D_{60}	D_{10}	Cu	Porosity	Re	Curve No.	Number of simulation	D_{60}	D_{10}	Cu	Porosity	Re
1	2	0.335	0.16	2.094	0.42	0.223	1	2	0.335	0.2	2.094	0.55	0.514
2	2	0.235	0.16	1.469	0.42	0.095	2	2	0.235	0.2	1.469	0.55	0.184
3	2	0.28	0.15	1.867	0.42	0.128	3	2	0.28	0.2	1.867	0.55	0.266
4	2	0.18	0.14	1.286	0.42	0.052	4	2	0.18	0.1	1.286	0.55	0.101
5	2	0.34	0.295	1.153	0.42	0.433	5	2	0.34	0.3	1.153	0.55	0.816
6	2	0.295	0.235	1.255	0.42	0.253	6	2	0.295	0.2	1.255	0.55	0.477

soils with rounded grains is of concern. After initialization, the LBM computational loop of advection and collision continues until steady-state condition is obtained. An example of the velocity field calculated with this method is shown in Fig. 5. Intrinsic permeability (k), which depends on packing configuration only, is analyzed for different conditions. k is calculated by the following relation:

$$\frac{dP}{dl} = \frac{\mu V}{k}, \tag{28}$$

where $\frac{dP}{dl}$ is the pressure gradient and μ is dynamic viscosity of the fluid. Discharge velocity (V) is obtained by averaging fluid velocities on a cross section lattice perpendicular to the flow direction. Darcy's law is valid if the flow through soil is laminar (slow-viscous flow), and this depends on the dimension of interstices which, in turn, depends upon the particle size. It has been found that flow through soil is laminar when Reynolds number is about unity or less thus it would be valid to apply Darcy's law. The Reynolds number (Re) for flow through porous media flow is typically expressed as [78]

$$\mathrm{Re} = \frac{V\mathrm{D}}{\upsilon}, \tag{29}$$

where D is average diameter of the porous media particles and υ is the fluid kinematic viscosity. Flow through soil with $\mathrm{Re} \lesssim 1$ is considered laminar and with $\mathrm{Re} \gtrsim 10$ is turbulent. Flow between these two limits is transient. The average Re number for each sample in this study is shown at Tables I and II.

In order to demonstrate the validity of the permeability values derived from the developed LBM code, here we present a comparison between the analytical solution and the LBM simulation results for calculation of permeability values for fluid flow through an idealized porous medium formed from periodic body centered cubic (BCC) array of spheres of equal radius a [Fig. 6(a)]. The permeability value for this idealized medium analytically can be derived as follows [23,24,36]:

$$k^* = \frac{V_0}{6\pi a d^*}, \quad d^* = \sum_{n=0}^{30} \alpha_n \chi^n, \tag{30}$$

$$\chi = \left(\frac{c}{c_{\max}}\right)^{1/3}, \quad c = \frac{4\pi a^3}{3V_0}, \quad c_{\max} = \frac{\sqrt{3}\pi}{8}, \tag{31}$$

where k^* is permeability, d^* is inverse of the dimensionless drag, $V_0 = \frac{1}{2}L^3$ where L is center to center distance of spheres, the coefficient α_n are given in [24], c is concentration of spheres, and $c_{\max}$ is the maximum concentration of spheres for given packing geometry. The spheres radius for each resolution is equal to $a = \sqrt{3}L\chi/4$ and the pore throat is $\eta = \sqrt{3}L(1-\chi)/2$ [36].

We evaluated the capability and precision of our MRT-LBM code in modeling of flow through porous media with various resolutions L^3, different viscosities, and different porosities.

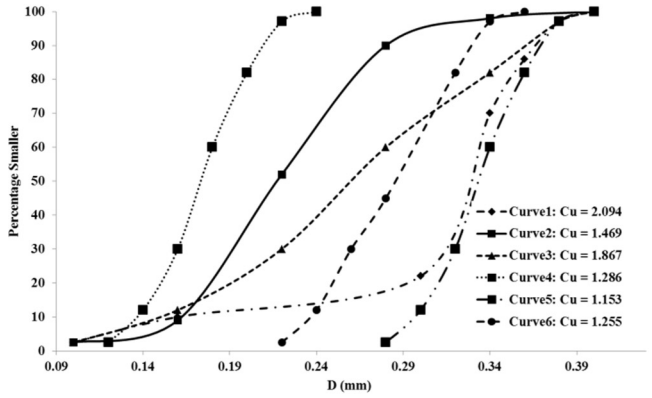

(a)

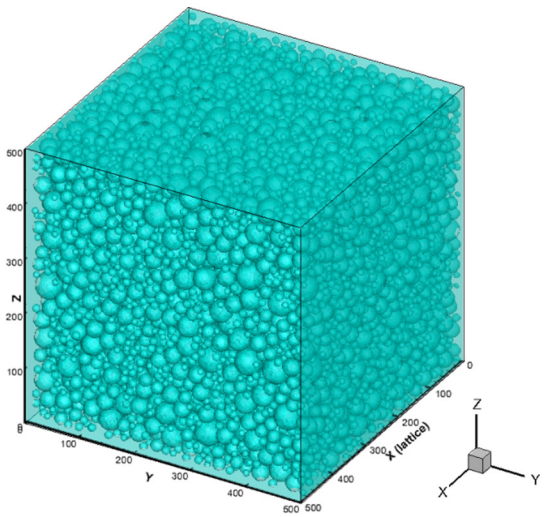

(b)

FIG. 4. (Color online) (a) Grain-size distribution of samples. (b) An example of nonhomogenized sample generated by DEM and introduced to LBM code.

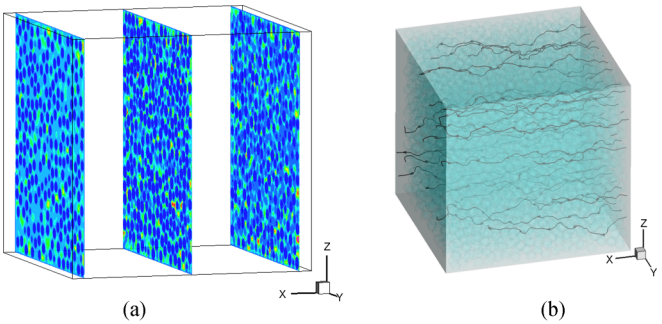

FIG. 5. (Color online) (a) Velocity magnitudes ($u^2 = u_x^2 + u_y^2 + u_z^2$) at three cross sections of the sample. (b) Streamlines generated with the constant-flux constraint for the same system as in (a).

In order to simulate BBC array of spheres, we considered domains with periodic boundary in all directions, and consider domains' obstacles as shown in Fig. 6(b) and 6(c), thereby we have domains equivalent to fully repetitive BCC pattern. Then in each domain we applied a body force along the x direction [Fig. 6(b)] and after the steady-state condition is reached we calculated the permeability.

Figure 7(a) shows the ratio of the simulated permeabilities (k) to analytical permeabilities (k^*), where we fixed the $\chi \approx 0.85$ and varied the resolution (L). According to this figure our LBM code shows excellent results. This figure indicates permeability becomes accurate and grid independence if $L > 16$ [36], it means that to see an object as a sphere in a lattice domain we need radius of 5.8 lattices or more. Based on Fig. 7(b) in the low resolutions we cannot make an obstacle similar to sphere, and since the above analytical solution is derived for sphere obstacles we get deviation between analytical and simulated results. In this figure also we examined the viscosity dependence (relaxation parameter) of the permeability by calculating permeabilities at $\tau = 0.55$ and 1.0 for the same domains. According to this figure viscosity has no effect on the permeabilities especially while we have obstacles that can be considered as spheres in the domain.

We next investigated the effect of porosity on the precision of MRT-LBM prediction regarding the permeability values. To do so we considered domains with $L = 50$ and $a = 10.8$, 13.0, 15.2, 17.3, 18.4, 19.5, 20.6, 21.0, and 22.0. According to Fig. 8 the normalized simulated permeabilities show excellent accuracy.

In order to illustrate the benefit of the MRT over BGK collision operator, we performed a simulation for flow through a homogeneous spherical particle pack. We calculated the steady-state Darcy velocity and estimated the saturated permeability of the medium with respect to different fluid viscosities. We performed this test for two different lattice sizes: $100 \times 100 \times 100$ and $200 \times 200 \times 200$ using both the MRT and BGK models. As shown in Fig. 9, the simulated permeability obtained by the BGK model increases significantly with increasing viscosities. As mentioned before, one major drawback of this operator with respect to the prediction of the permeabilities is that the exact position of the modeled fluid-solid interface changes if the lattice viscosity changes. This causes an apparent viscosity dependence of the predicted permeability while permeabilities obtained by the MRT model remain constant. Similar results are reported by Refs. [36,65,77].

As presented above, the MRT approach to LBM provides significant capability in simulation of flow through porous media in comparison to BGK-LBM. However, some researchers have opened new possibilities into BGK-LBM, for example, by regularizing the precollision distribution functions in order to achieve better stability and accuracy at very low computational cost [79]. Furthermore, researchers in Ref. [80] have developed a two-relaxation-time (TRT) LBM with variable source terms based on equivalent equilibrium functions. They derived a special parametrization of the free relaxation parameter and have claimed that when the boundary scheme obeys the parametrization properly, the derived permeability values become independent of the selected viscosity for any porous structure and can be computed efficiently.

A. Total and effective porosities

As mentioned, various equations relating the permeability of soils to its porosity have been proposed. In order to study the effects of the void ratio or porosity on intrinsic permeability, a series of samples with monosized solid particles and different porosities were simulated. In these analyses, particles' diameter was fixed to be 1.2 mm and the porosity is calculated as the number of pixels representing pore space divided by the total

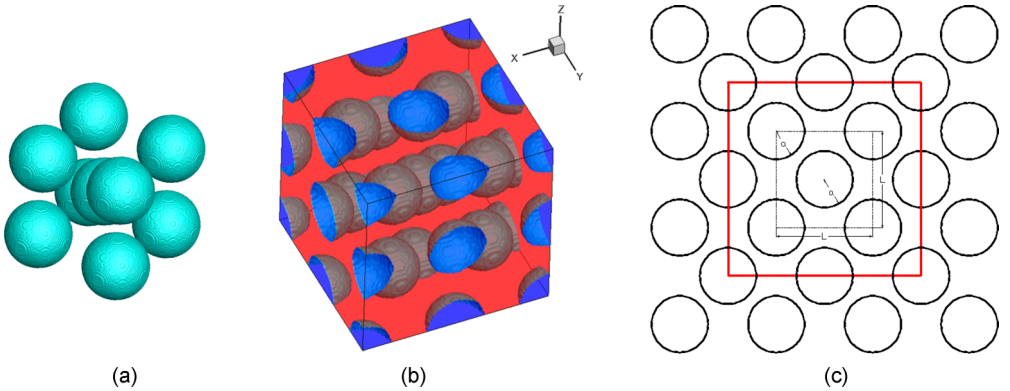

FIG. 6. (Color online) (a) BCC pattern of spheres. (b) An example of the BCC periodic domain considered for simulation. (c) 2D projection of BCC array of spheres; the red lines show the domain boundaries considered in (b).

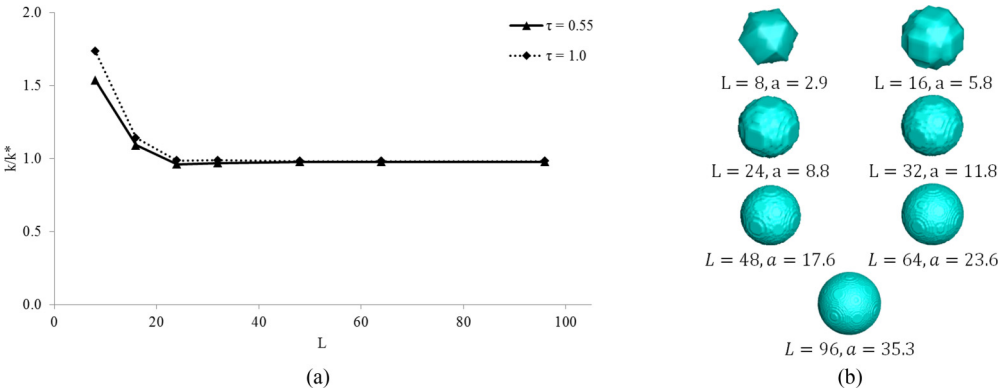

FIG. 7. (Color online) (a) Normalized permeability as a function of grid resolution L for $\chi \approx 0.85$. (b) Spheres made with different radii in lattice.

number of pixels in the 3D sample. In Fig. 10, variation of normalized intrinsic permeabilities (k/d_p^2) versus porosity is shown. As can be seen, there is a very good agreement between LBM results and other empirical and analytical equations for porosities greater than 0.5, especially, excellent agreement with Kozeny-Carman [Eq. (7)].

An interesting aspect of Fig. 10 occurs at the porosities less than 0.5, which to the contrary of all proposed equations, LBM simulations have predicted greater slope indicating decreasing permeability due to decreasing the porosity of porous media. Such behavior was also reported in Ref. [43]. As discussed earlier, it could be related to dead-end and no connecting pores in porous media. It means that, although pores exist in low porosities, but they may not be connected to each other and do not contribute to fluid flow in the porous media. This fact which occurs in low porosities does not seem to be considered in analytical relations. Figure 11 shows the numerically derived ϕ_{eff} versus the porosity. A dashed line is fitted to the simulated ϕ_{eff} values. For calculating ϕ_{eff} of different samples only the streamlines that pass through the whole length of the sample are considered, and the tortuosities are calculated using the method described in Ref. [47].

According to Fig. 11 the percolation threshold is about $\phi_c = 0.35$. It means that the samples with the porosity less than the percolation threshold will have effective porosity about $\phi_{\text{eff}} = 0.0$. Therefore, these samples have no permeability at all. Koponen *et al.* [43] proposed the following correlation between ϕ_{eff} and ϕ:

$$\phi_{\text{eff}} = ax^3 - (2a + \phi_c)x^2 + (a + 1 + \phi_c)x, \tag{32}$$

where $x = (\phi - \phi_c)/(1 - \phi_c)$ and the parameter a is a fitting value. Although this equation satisfies the conditions $\phi_{\text{eff}} = d\phi_{\text{eff}}/d\phi = 1$ at $\phi = 1$, and $\phi_{\text{eff}} = 0$ at $\phi = \phi_c$, there is some difficulties in determining appropriate fitting value and also ϕ_c. In addition, Koponen et al. proposed this correlation for their 2D simulations and it cannot reproduce our results from 3D simulations. We propose the following expression which gives a good quantitative estimate of the simulated results:

$$\phi_{\text{eff}} = a \ln(\phi) + 1.0, \tag{33}$$

where a is a fitting parameter which here can be assumed $a = 0.93$. According to Fig. 12 we can see an improvement in the results of Kozeny-Carman [Eq. (7)] when the porosity is replaced by the effective porosity [Eq. (8)]. In order to employ Eq. (8) we have used effective porosity calculated from Eq. (33). The solid line shown in Fig. 12 is plotted based on the proposed equation as below:

$$k/d_p^2 = \frac{\phi_{\text{eff}}^5}{(1 - \phi_{\text{eff}})^2(1 + \phi_{\text{eff}})^8} \tag{34}$$

or

$$k/d_p^2 = \frac{[1.0 + a \ln(\phi)]^5}{(a \ln(\phi))^2[2.0 + a \ln(\phi)]^8}. \tag{35}$$

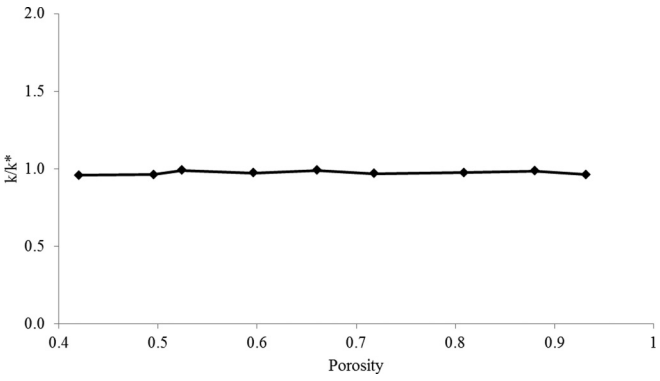

FIG. 8. Normalized permeability as a function of porosity.

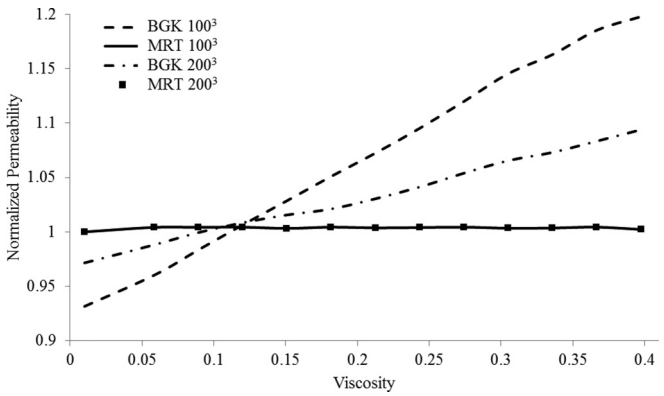

FIG. 9. Comparison of the calculated permeabilities using the BGK and MRT operators.

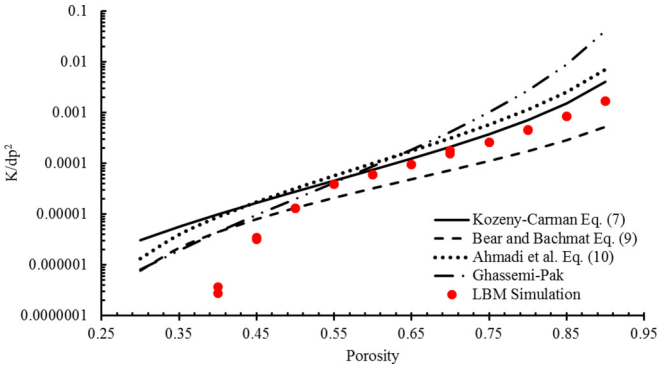

FIG. 10. (Color online) Variations of intrinsic permeability versus porosity.

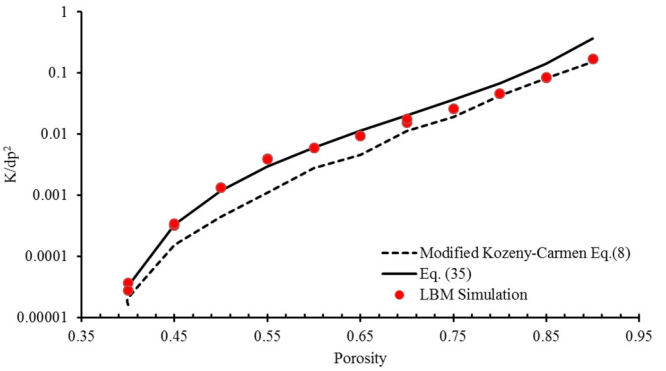

FIG. 12. (Color online) Normalized permeability as a function of porosity for monosized samples ($d_p = 1.2$ mm).

B. Particles' size

It has generally been recognized by the previous investigators that the particle size is a fundamental independent variable controlling the permeability [81–83]. Consider a simple power equation of the form

$$k = ad_p^b, \tag{36}$$

where k is permeability, a is a constant usually accounts for tortuosity, porosity of medium, and mathematical dimension or in general can be taken to include all factors intrinsic to the medium that affect the permeability except the size, and d_p is either pore throat or a representative particle diameter [84]. A review of the literature reveals few studies that have proposed this power equation with different a and b values to describe the relationship between particle size and permeability. For example, for hydraulic conductivity (GPD/ft^2) several researchers proposed the following quantities for a and b: Hazen [85] ($a = 1.50$, $b = 1.60$), king [86] ($a = 11.90$, $b = 1.56$), Muskat [87] ($a = 12.39$, $b = 1.84$), Bedinger [88] ($a = 1.01$, $b = 1.47$), and Burmister [89] ($a = 18.35$, $b = 1.95$). It should be mentioned that although Eq. (36) have been extensively used as a general form to relate the permeability to the size of the particles, the dimensions of both sides of the equation should match. In this regard, we must assume the "a" factor has a proper dimension with respect to the power of "b" so that Eq. (36) becomes mathematically correct. For example, based on the results of the numerical simulations conducted in this investigation we obtained the following empirical relation for $\phi = 0.5$:

$$k \cong 0.0005 d_p^{1.47} (\text{cm}^2). \tag{37}$$

On the other hand, soil is composed of particles with different sizes. In addition, smaller particles have more influence on the coefficient of permeability due to their greater specific surface area. Hence, extensive investigations have been conducted on correlating the permeability with fraction of fine grains (D_{10}, D_5, and coefficient of uniformity $\text{Cu} = D_{60}/D_{10}$) in the soil. For example, Ref. [90] developed a permeability formula in which

$$k \propto D_{60}^{0.6} D_{10}^{1.72} \left[\frac{\phi^3}{1+\phi} \right]. \tag{38}$$

To study this, several soil samples with different grain-size distributions as depicted in Fig. 4 , are considered. Soil samples for each of the grain-size distributions were prepared with two porosities $\phi = 0.42$ and $\phi = 0.55$. The normalized intrinsic permeability (k/D_{10}^2) of LBM simulations of these samples are calculated and plotted versus Cu in Fig. 13. The results show that the permeability depends on the coefficient of uniformity of the samples and increases with increasing uniformity coefficient almost with a linear trend. It is in agreement with the results of Ref. [57] and somewhat opposite to the results of laboratory studies by Ref. [91] on the permeability of granular filters, which indicate that uniformity coefficient has little

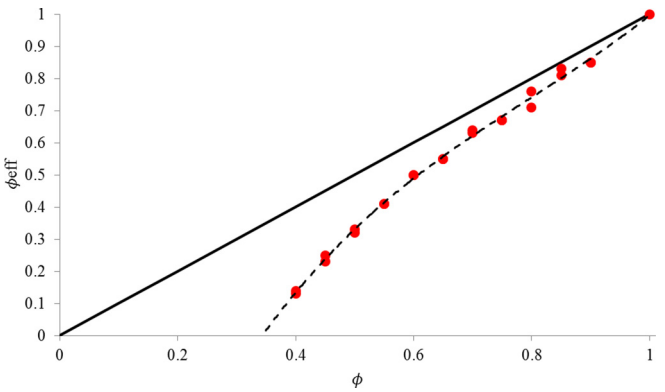

FIG. 11. (Color online) The simulated effective porosity vs porosity.

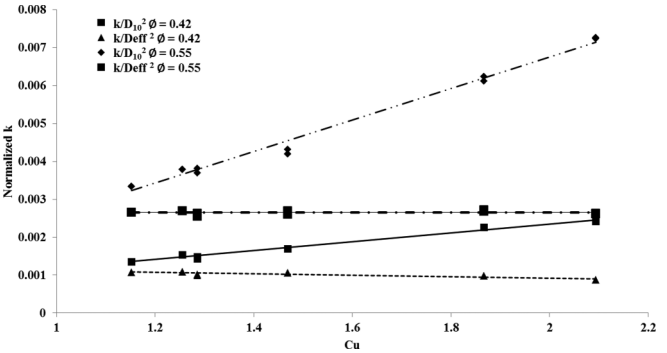

FIG. 13. Variations of normalized intrinsic permeability against uniformity coefficient.

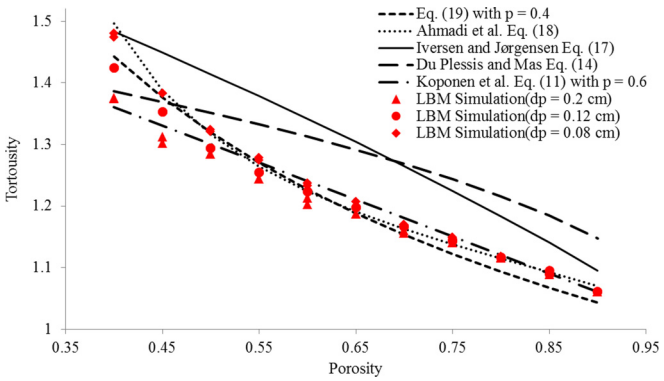

FIG. 14. (Color online) Variation of tortuosity versus porosity for three particle diameters.

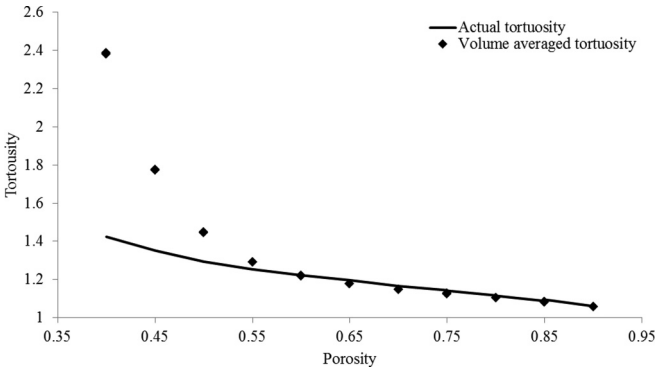

FIG. 15. Comparing actual tortuosity and volume-averaged tortuosity.

influence on the permeability in comparison with the influence of the percentage of smaller particles.

If the soil consists of nonuniform spheres, the effective diameter D_{eff} taken from the particle size distribution can substitute d_p value. In this work, "effective diameter" as defined in Ref. [92] is considered as a representative parameter for specific surface area of the sample:

$$D_{\text{eff}} = \frac{100\%}{\sum^{f_\chi} / D_{\text{ave},\chi}}, \tag{39}$$

where χ represents number of the particle size classes that are used, and f_χ shows fraction of the particles between two sieves larger ($D_{l,\chi}$) and: smaller ($D_{s,\chi}$), calculated by:

$$D_{\text{ave},\chi} = \sqrt{D_{l,\chi} D_{s,\chi}}. \tag{40}$$

The variation of the normalized permeability (k/D_{eff}^2) with uniformity coefficient of the samples with various porosities is depicted in Fig. 13. The figure shows that there is a strong correlation between permeability and effective diameter. By using the effective diameter for predicting the permeability coefficient, the effects of uniformity coefficient are implicitly accounted for. Hence, the effect of Cu on the permeability almost disappears in this way.

C. Tortuosity

As mentioned before, another important parameter which affects fluid flow in the porous media and as a result, the intrinsic permeability, is the tortuosity of streamlines in the porous media. In Fig. 14 LBM simulation results along with the proposed equations have been presented. This figure demonstrates the reduction of the tortuosity of the flow paths with increasing the porosity for monosized samples as defined by Eq. (3). The trend of the data can roughly be considered linear similar to that proposed by Koponen *et al.* [Eq. (11)] or the equation proposed by Iversen and Jørgensen [Eq. (17)], but contradictory to the nonlinear relations given by some other researchers. As we can see, the simulations results have an excellent agreement with the equation proposed by Ahmadi *et al.* [Eq. (18)] especially for porosities greater than 0.55. In addition, the simulation results have a good agreement with the simple Eq. (19) proposed by different authors.

In Fig. 15 the actual tortuosity is compared with the "volume-averaged tortuosity" [57,81], whose definition is

$$T = \frac{\sum |V(x,y,z)|}{\sum |V_i(x,y,z)|}, \tag{41}$$

where $|V_i(x,y,z)|$ is the magnitude of velocity in the direction i along which the pressure gradient is applied, and $|V(x,y,z)|$ is the magnitude of velocity vector at a certain location with the coordinates of (x, y, z):

$$|V(x,y,z)| = \sqrt{V_x(x,y,z)^2 + V_y(x,y,z)^2 + V_z(x,y,z)^2}. \tag{42}$$

As can be seen in this Fig. 15, the volume-averaged tortuosity tends to very large values for the porosities less than 0.55 and tends to infinity at positions where velocity in the direction i is close to zero. Also in Eq. (12) when the porosity gets close to ϕ_c, the tortuosity tends to infinity. This does not seem to actually occur in 3D porous media such as granular soils. When the porosity gets close to ϕ_c the streamlines which successfully reach the end of the domain become less and less until no complete streamline remains, and it does not mean that tortuosity must tend toward very large values. As shown in Fig. 15 the actual tortuosity does not become very large even at low porosities.

In Fig. 14 the simulation results for three different particle diameters have also been presented. According to this graph, tortuosity decreases with greater particle diameters, but particle diameters in the range of sandy soils do not affect the tortuosity parameter very much, especially for porosities greater than 0.6.

V. CONCLUSION

A newly developed 3D multirelaxation time LBM code has been employed to investigate the effects of several issues such as effective porosity, particle size, pore size distribution, and tortuosity on the infiltration characteristics of saturated granular media. Different soil samples have been made numerically using the Discrete Element Method. The study highlights the importance of considering three dimensionality of the flow regime in order to obtain a realistic view regarding

the streamlines and the effects of tortuosity on the permeability of the granular soil strata.

From the LBM simulations conducted in this study the following conclusion can be drawn:

(1) In granular soils, there exists a "threshold porosity" below which, the connectivity of the pore spaces in the soil virtually vanishes and the permeability of the soil drastically reduces.

(2) To take the occluded pore spaces and dead-end stream paths into account it is recommended to use effective porosity value ($\emptyset_{\text{eff}}$) instead of the total porosity in the commonly used relationships proposed for estimating the soil permeability. Excellent logarithmic fits were found to the simulated results, but it was not possible to deduce simple analytical expressions for nonhomogenized samples.

(3) Variations of the normalized permeability with respect to the D_{10} shows a linear increasing trend when it is plotted against the coefficient of uniformity (Cu), and it becomes constant when it is plotted using D_{eff} of the soil.

(4) The tortuosity value has a general decreasing trend when the soil porosity or particles diameters increase, however, due to 3D mechanism of the flow even for low porosities, it does not become higher than 1.6. Also, the numerical results show that the porosity has greater effects on tortuosity comparing to particle diameter for the diameters in a range of sandy soils.

(5) In contrast with volume average tortuosity, the actual tortuosity does not tend towards infinity at the porosities close to the threshold porosity (ϕ_c).

[1] M. Sahimi, Rev. Mod. Phys. **65**, 1393 (1993).
[2] S. T. Han, Pulp Paper Mag. Can. **70**, T134 (1969).
[3] G. W. Jackson and D. F. James, Can. J. Chem. Eng. **64**, 364 (1986).
[4] K. H. Hellmuth, P. Klobes, K. Meyer, B. Rohl-Kuhn, M. Siitari-Kauppi, J. Hartikainen, K. Hartikainen, and J. Timonen, Z. Geol. Wiss. **23**, 691 (1995).
[5] D. L. Johnson, J. Koplik, and L. M. Schwartz, Phys. Rev. Lett. **57**, 2564 (1986).
[6] S. Kostek, L. M. Schwartz, and D. L. Johnson, Phys. Rev. B **45**, 186 (1992).
[7] A. J. Katz and A. H. Thompson, J. Geophys. Res. B **92**, 599 (1987).
[8] D. J. Wilkinson, D. L. Johnson, and L. M. Schwartz, Phys. Rev. B **44**, 4960 (1991).
[9] A. H. Thompson, S. W. Sinton, S. L. Huff, A. J. Katz, R. A. Raschke, and G. A. Gist, J. Appl. Phys. **65**, 3259 (1989).
[10] D. L. Johnson, D. L. Hemmick, and H. Kojima, J. Appl. Phys. **76**, 104 (1994).
[11] A. E. Scheidegger, *The Physics of Flow through Porous Media* (Macmillan, New York, 1957).
[12] J. Bear, *Dynamics of Fluids in Porous Media* (Dover, New York, 1972).
[13] F. A. L. Dullien, *Porous Media. Fluid Transport and Pore Structure* (Academic, San Diego, 1979).
[14] J. Bouma, A. Jongerius, O. Boersma, A. Jager, and D. Schoonderbeek, Soil Sci. Soc. Am. J. **41**, 945 (1977).
[15] H. J. Vogel and U. Babel, Experimental Relationship between the Morphological Pore-Size Distribution and the Soil Water-Retention Characteristic, in *Soil Micromorphology: Studies in Management and Genesis*, edited by A. J. Ringrose-Voase and G. S. Humphreys, Proceedings of the IX International Working Meeting on Soil Micromorphology, Townsville, Australia, July 1992. Developments in Soil Science 22 (Elsevier, Amsterdam, 1994), pp. 591–600.
[16] M. Kaviany, *Principles of Heat Transfer in Porous Media* (Springer-Verlag, New York, 1991).
[17] R. P. Chapuis and M. Aubertin, Can. Geotech. J. **40**, 616 (2003).
[18] D. Hansen, Can. Geotech. J. **41**, 990 (2004).
[19] R. P. Chapuis and M. Aubertin, Can. Geotech. J. **41**, 994 (2004).
[20] J. K. Mitchell and K. Soga, *Fundamentals of Soil Behavior* (Wiley, New York, 2005).
[21] Y. Mualem, Water Resour. **12**, 2187 (1976).
[22] K. Kosugi, Soil Sci. Soc. Am. J. **63**, 270 (1999).
[23] H. Hasimoto, J. Fluid Mech. **5**, 317 (1959).
[24] A. S. Sangani and A. Acrivos, Int. J. Multiphase Flow **8**, 343 (1982).
[25] I. W. Crawford, Eur. J. Soil Sci. **45**, 493 (1994).
[26] T. Abichou, C. H. Benson, and T. B. Edil, Can. Geotech. J. **41**, 698 (2004).
[27] X. Zhang, L. K. Deeks, A. G. Bengough, J. W. Crawford, and I. M. Younga, J. Hydrol. **306**, 59 (2005).
[28] S. Chen and G. Doolen, Annu. Rev. Fluid Mech. **30**, 329 (1998).
[29] S. Succi, E. Foti, and F. Higuera, Europhys. Lett. **10**, 433 (1989).
[30] D. H. Rothman, Geophysics **53**, 509 (1988).
[31] A. Cancelliere, C. Chang, E. Foti, D. H. Rothman, and S. Succi, Phys. Fluids A **2**, 2085 (1990).
[32] M. Sahimi and D. Stauffer, Chem. Eng. Sci. **46**, 2225 (1991).
[33] S. Chen, K. Diemer, G. D. Doolen, K. Eggert, C. Fu, S. Gutman, and B. J. Travis, Physica D **47**, 72 (1991).
[34] U. Brosa and D. Stauffer, J. Stat. Phys. **63**, 405 (1991).
[35] J. Kim, J. Lee, and K. Lee, Physica A **293**, 13 (2001).
[36] C. Pan, L. Luo, and C. Miller, Comput. Fluids **35**, 898 (2006).
[37] A. W. J. Hejis, and C. P. Lowe, Phys. Rev. E **51**, 4346 (1995).
[38] J. Kozeny, Math.-naturwissenschaft. Klasse (Abt. IIa **136**, 271 (1927).
[39] P. C. Carman, Trans. Inst. Chem. Eng. **15**, 150 (1937).
[40] P. C. Carman, *Flow of Glass Through Porous Media* (Butterworths, London, 1956).
[41] M. Matyka, A. Khalili, and Z. Koza, Phys. Rev. E **78**, 026306 (2008).
[42] J. Bear, *Dynamics of Fluids in Porous Media* (Elsevier, New York, 1972).
[43] A. Koponen, M. Kataja, and J. Timonen, Phys. Rev. E **56**, 3319 (1997).
[44] M. Kaviany, *Principles of Heat Transfer in Porous Media,* 2nd ed. (Springer, New York, 1995).
[45] J. Bear and Y. Bachmat, *Introduction to Modeling of Transport Phenomena in Porous Media* (Kluwer Academic, Dordrecht, 1990).

[46] M. M. Ahmadi, S. Mohammadi, and A. N. Hayati, Phys. Rev. E **83**, 026312 (2011).
[47] A. Koponen, M. Kataja, and J. Timonen, Phys. Rev. E **54**, 406 (1996).
[48] H. L. Weissberg, Appl. Phys. **34**, 2636 (1963).
[49] E. Mauret and M. Renaud, Chem. Eng. Sci. **52**, 1807 (1997).
[50] J. P. Du Plessis and J. H. Masliyah, Transp. Porous Media **6**, 207 (1991).
[51] B. P. Boudreau, Geochim. Cosmochim. Acta **60**, 3139 (1996).
[52] J. Comiti and M. Renaud, Chem. Eng. Sci. **44**, 1539 (1989).
[53] N. Iversen and B. B. Jørgensen, Geochimica et Cosmochim. Acta **57**, 571 (1993).
[54] F. A. L. Dullien, Chem. Eng. J. **10**, 1 (1975).
[55] M. Mota, J. A. Teixeira, and A. Yelshin, Trans. Filtr. Soc. **1**, 101 (2001).
[56] R. Dias, M. Mota, J. A. Teixeira, and A. Yelshin, Filtration **5**, 68 (2005).
[57] A. Ghassemi and A. Pak, Int. J. Num. Anal. Meth. Geomech. **35**, 886 (2011).
[58] H. Chen, S. Chen, and W. H. Matthaeus, Phys. Rev. A **45**, R5339(R) (1992).
[59] Y. H. Qian, D. d'Humières, and P. Lallemand, Europhys Lett. **17**, 479 (1992).
[60] D. d'Humières, Prog. Astronaut Aeronaut Washington (DC) **159**, 450 (1992).
[61] P. Lallemand and L. S. Luo, Phys. Rev. E **61**, 6546 (2000).
[62] A. G. Yiotis, J. Psihogios, M. E. Kainourgiakis, A. Papaioannou, and A. K. Stubos, Physicochem. Eng. Aspects **300**, 35 (2007).
[63] D. d'Humières, I. Ginzburg, M. Krafczyk, P. Lallemand, and L. S. Luo, Philos. Trans. R. Soc. London, Ser. A **360**, 437 (2002).
[64] R. Mei, L. Luo, P. Lallemand, and D. d'Humières, Comput. Fluids **35**, 855 (2006).
[65] M. L. R. Thomas, D. B. Ingham, and M. Pourkashanian, Open Transport Phenomena J. **2**, 80 (2010).
[66] Y. T. Feng, K. Han, and D. R. Owen, Int. J. Num. Methods Eng. **72**, 1111 (2007).
[67] S. Succi, *The Lattice-Boltzmann Equation for Fluid Dynamics and Beyond* (Clarendon Press, Oxford, 2001).
[68] M. C. Sukop and D. T. Thorne, Jr., *Lattice Boltzmann Modeling: An Introduction for Geoscientists and Engineers*, 2nd ed. (Springer, New York, 2007).
[69] M. Hecht and J. Harting, J. Stat. Mech. (2010) P01018.
[70] P. A. Cundall and O. D. L. Strack, Geotechnique **29**, 47 (1979).
[71] Itasca, PFC2D 2.00 User Manual, Itasca Consulting Company (Minneapolis, Minnesota, 1998).
[72] P. Thomas, Ph. D. thesis, University of California, Berkeley, 1997.
[73] J.-A. Ferrez, Ph. D. thesis, Ecole Poly technique Federal de Lausanne, Lausanne, 2001.
[74] C. O'Sullivan, Ph. D. thesis, University of California, Berkeley, 2002.
[75] L. Cui and C. O'Sullivan, Granular Matter **5**, 135 (2003).
[76] S. Succi, *The Lattice Boltzmann Equation for Fluid Dynamics and Beyond* (Clarendon Press, New York, 2001).
[77] A. Narváez, K. Yazdchi, S. Luding, and J. Harting, J. Stat. Mech. (2013) P02038.
[78] B. M. Das, *Advanced Soil Mechanics*, 3rd ed. (Taylor & Francis, New York, 2008).
[79] J. Latt and B. Chopard, Math. Comput. Simulation **72**, 165 (2006).
[80] I. Ginzburg, F. Verhaeghe, and D. d'Humières, Commun. Comput. Phys. **3**, 427 (2008).
[81] L. C. Graton and H. J. Fraser, J. Geol. **43**, 795 (1935).
[82] B. P. Reyes, Philippine Geol. **20**, 93 (1966).
[83] N. R. Morrow, J. D. Huppler, and A. B. Simmons, J. Sediment. Petrol. **39**, 312 (1969).
[84] R. G. Shepherd, Ground Water **27**, 633 (1989).
[85] A. Hazen, Some Physical Properties of Sands and Gravels, with Special Reference to Their Use in Filtration, in *Massachusetts State Board of Health*, 24th Annual Report. Publication No. 34, pp. 539–556 (1892).
[86] F. H. King, U.S. Geol. Surv. 19th Ann. Rept. **2**, 59 (1899).
[87] M. Muskat, J. W. Edwards Inc. **15**, 113 (1937).
[88] M. S. Bedinger, U. S. Geol. **424**, 31 (1961).
[89] D. M. Burmister, American Society for Testing and Materials **163**, 3 (1954).
[90] A. M. Amer and A. A. Awad, J. Geotech. Eng. Div., Am. Soc. Civ. Eng. **100**, 1309 (1974).
[91] T. Kenney, D. Lau, G. Ofoegbu, Can. Geotech. J. **21**, 726 (1984).
[92] W. D. Carrier, Geotech. Geoenviron. Eng. **129**, 1054 (2003).